Rosenblad, J. (1968). "Development of a rocklike model material". Proc. 10th symposium on rock mechanics, Austin, Texas, PP. 331 – 361.

Rowe, R.K. and Armitage, H.H. (1987 b) "A design method for drilled piers in soft rock" Canadian geotechnical journal. Vol. 24, PP. 126 –142.

Rosenberg, P. and Journeaux, N., (1976) "Friction and end bearing tests on bedrock for high capacity socket design" Canadian Geotechnical journal, Vol. 13, PP. 324 - 332.

Stimpson, B. (1970). "Modelling materials for engineering rock mechanics". International journal in rock mechanics and mining science, Vol. 7, PP. 77 – 121.

Williams, A. F. and Pells, P.J.N. (1981) "Side resistance rock sockets in sandstone, mudstone, and shale" Canadian geotechnical journal. Vol. 18. PP. 502 –513.

of load (Qb/ Qt) being carried to the base of the socket in the elastic range to be determined. These experiments show a higher ratio of load (Qb/ Qt) being carried to the base of the socket in case of experiments 2, 4, 11, which is 36 %, 27 %, 34 % respectively, compared with the 18 %, predicted by the elastic solution, and similar value in both cases for experiment 3 which is 19 %. The distribution of the shear stress predicted by the finite element programme compared well with that recorded in the laboratory experiments.

8. Recommendations for future work

1. It is possible to extend this research to study the effect of orientation and shape of the rock joints. This can be done by making the simulated materials with joints. Also, it is possible to study the effect of multiple beds
2. This research could be extended to study rock socketed piles in tension.

9. REFERENCES

Brown, E.T. (1981). "Rock characterization testing and monitoring, I.S.R.M. suggested methods". Published for the commission on testing methods international society for rock mechanics.

Horvath r. G., Kenny, T. C. and Kozicki, P. (1983) "Methods of improving the performance of drilled piers in weak rock" Canadian geotechnical journal Vol. 20, PP. 758-772.

Lam, T. S. K. and Johnston, I. W. (1989) "Shear behaviour of regular triangular concrete/ rock joints-evaluation" Geotechnical engineering, Vol. 115. 5, A.S.C.E., PP. 728 – 740.

Lama R. D., and, Vutukuri, V. S. (1978 a). "Hand book on mechanical properties of rocks" Volume I, Trans tech publications Clausthal, Germany.

Table 7.5. Comparison between the empirical relationships and the results of side shear stress.

↑. Mobilized Shear stress

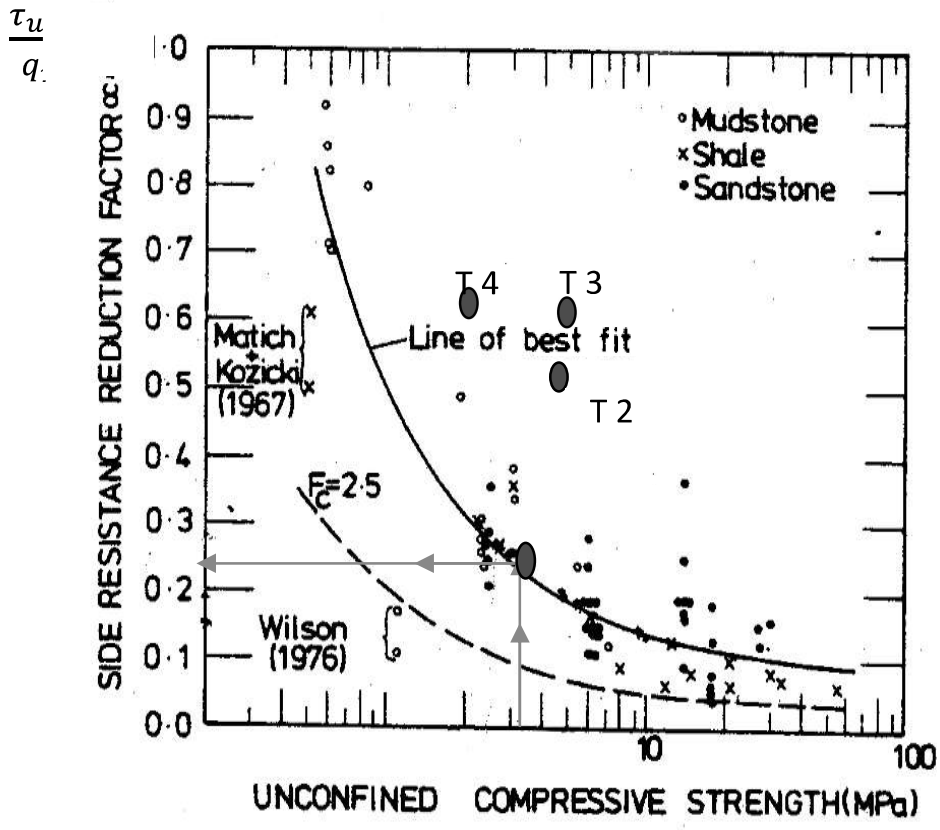

Figure 25. Correlation between the adhesion factor in the experiments results and that predicted by Williams and Pells (1981).

The maximum end bearing resistance was mobilized in four of the experiments. These showed that the relationship between maximum end bearing resistance, and the unconfined compressive strength, varied between 1.5 to 5.5 times the unconfined compressive strength which corresponds to a bearing capacity factor (Nc) factor of 3 to 10.95. These compare to a bearing capacity factor (Nc) value of 9 sometimes used in pile design. The load distribution along the shaft was obtained only in four experiments. This allowed the end bearing capacity and the ratio

reach the failure the mobilized adhesion factor was lower than the values predicted by the empirical relationship.

Exp. No	qr (MPa	Side shear stress (MPa)						Peak shear stress MPa	Adhesion factor, alpha α
		Rowe and Armitage 1987 b		Rosenberg and Journeaux 1976	Williams and Pells 1981		Horvath et al 1983		
		0.45 Smooth	0.60 Rough	(MPa)	α	αqr	0.25 Smooth		
1	9.24	1.37	1.82		0.15	1.39	0.76	-	-
2	4.85	0.99	1.32	-	0.21	1.02	0.55	2.5	0.515
3	5.32	1.04	1.38	-	0.20	1.06	0.58	3.31	0.622
4	2.10	0.65	0.87	0.55	0.33	0.69	0.36	1.33	0.633
5	2.90	0.77	1.02	-	0.28	0.81	0.43	-	-
6	2.43	0.70	0.93	-	0.29	0.70	0.39	-	-
7	3.55	0.85	1.13	-	0.24	0.85	0.47	-	-
8	2.47	0.71	0.94	-	0.29	0.72	0.39	0.76 ↑	3.80↑
9	22.75	2.15	2.86	1.86	0.10	2.28	1.19	0.83 ↑	0.60↑
10	2.54	0.72	0.96	-	0.29	0.74	0.40	0.34 ↑	1.10↑
11	3.80	0.88	1.17	-	0.23	0.87	0.49	0.84	0.221
12	1.37	0.53	0.70	0.45	0.47	0.64	0.29	0.46 ↑	0.336
13	6.81	1.17	1.57	-	0.18	1.23	0.65	0.45 ↑	0.066
14	3.02	0.78	1.04	-	0.25	0.76	0.43	0.68 ↑	2.30↑
15	5.09	1.02	1.35	0.93	0.20	1.02	0.56	1.1 0 ↑	6.60↑
16	8.44	1.31	1.74	1.13	0.15	1.26	0.73	0.97 ↑	4.47↑

Table 4. Mobilized shear stress and the mobilized end bearing for experiments 8,9,10,12,13,14,15,16.

The empirical relationships given by (Rosenberg and Journeaux 1976, Rowe and Armitage 1987 b, Williams and pells, Horvath et al 1983) for the prediction of peak shear stress is given in Table 5. The results of the four experiments in which the adhesion factor was determined are shown in Figure 25 below. Experiment 11, which has a smooth socket, is in a good agreement with the peak shear stress predicted by the empirical methods for the smooth socket, Whereas the experiments, 2, 3, and 4 which have rough sockets have higher adhesion factors compared with the empirical relationship predictions by Williams and Pells (1981) as shown in Figure 25. This difference could be related to the effect of discontinuities such as joints and fractures in the natural rock which were not modelled in the experiments, and also could be due to scale effects.

7. Conclusions

Laboratory experiments of micropiles in synthetic rock are considered to have successfully modelled rock socketed piles in the intact rock mass. Useful information regarding the shaft resistance mobilized can be obtained from such experiments, and this could be developed further by introducing layered synthetic rock systems and discontinuities (joint systems, fractures) within the synthetic rock.

The adhesion factor was determined at the maximum average shear stress in four experiments, and in eight experiments at the mobilized shear stress. The adhesion factor at the maximum average shear stress was about 0.6 in the rough socket, which is higher than the values predicted by the empirical relationships. This difference could be related to the effect of the discontinuities in the natural rock, which were not modelled in the experiments, and also due to scale effects. In case of the smooth socket the adhesion factor was 0.22, which is the same value predicted by the empirical relationship for the smooth socket. In the case of the pile experiments which did not

shows good agreement between the finite element analysis and the experiment results with maximum shear stress 1.64 MPa. at 14 kN applied load.

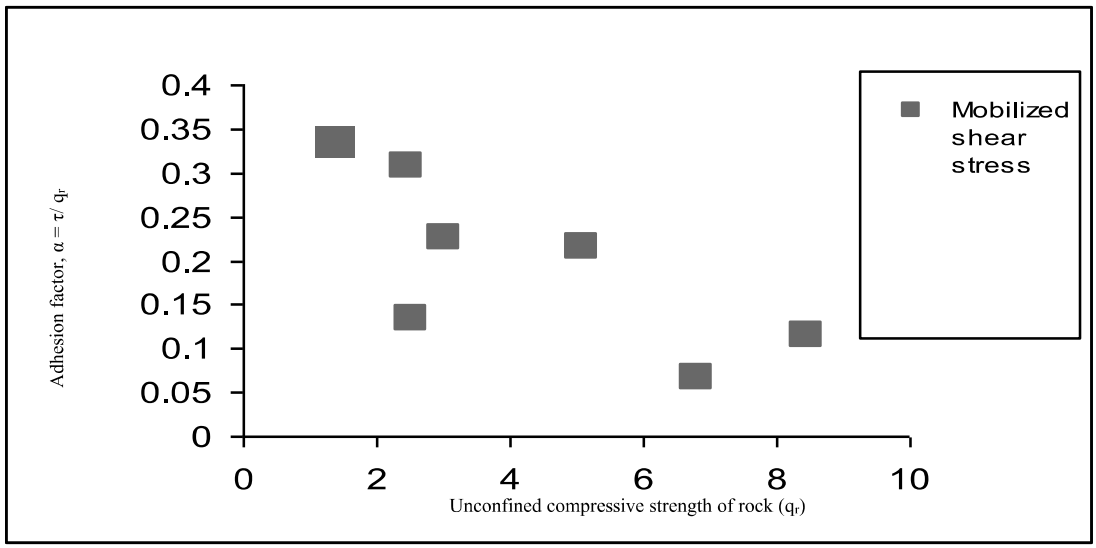

Figure 24. Correlations between the unconfined compressive strength with the adhesion factor, (α).

Exp. No.	The unconfined compressive strength (qr) (MPa)	Mobilized shear stress (Experimental) MPa	The experiments adhesion factor. α = τ/ qr	Mobilized base stress MPa	Ratio between qr and the mobilized end bearing stress
8	2.47	0.76	0.308	3.80	1.54
9	22.75	0.83	0.037	0.60	0.026
10	2.54	0.34	0.134	1.10	0.433
12	1.37	0.46	0.336	3.50	2.55
13	6.81	0.45	0.066	1.80	0.264
14	3.02	0.68	0.225	2.30	0.762
15	5.09	1.1 0	0.216	6.60	1.30
16	8.44	0.97	0.115	4.47	0.529

Table 3. The maximum average shear stress, the maximum end bearing, and their relation to the unconfined compressive strength of rock.

The mobilized shear stress and the mobilized end bearing were determined in eight experiments in which the total loads – displacement curve was not completed because of the pile head failure as shown in Table 4. The mobilized adhesion factor (α), the mobilized shear stress, mobilized base stress and the ratio between the unconfined compressive strength and the mobilized end bearing stress for these eight experiments are also given in Table 4. The comparison between the mobilized adhesion factor (α) and the unconfined compressive strength is shown in Figure 24. These experiments confirm (as shown in Table 5) that the mobilized average shear stress is lower than the values to be expected by the empirical relationships.

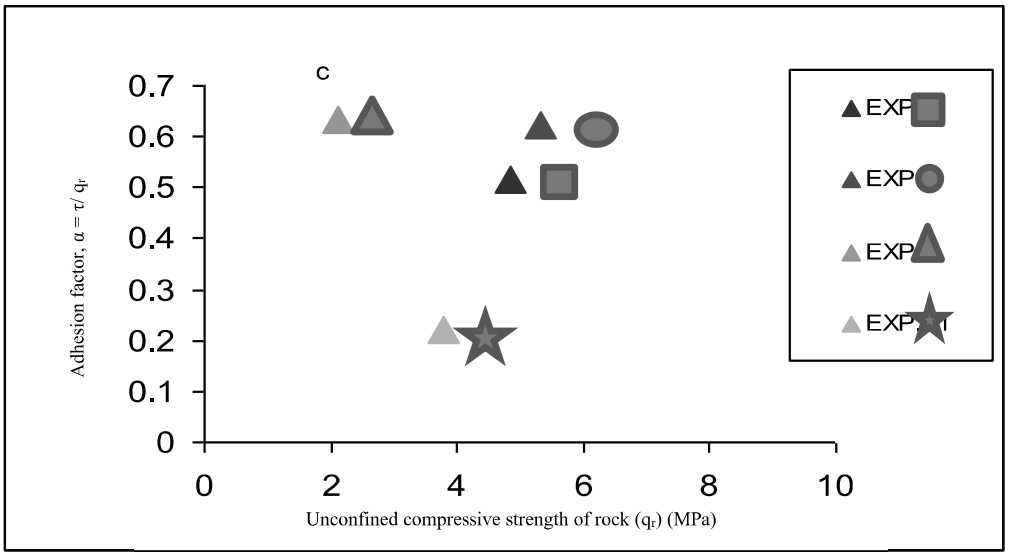

Figure 23. Correlations between the unconfined compressive strength with the adhesion factor, (α).

The shear stress distribution along the shaft was only reliably measured in experiment No. 11 (smooth pile). This experiment

Figure 22. A comparison between the final shear stress profiles that produced by finite element analysis and the experiments result in experiment 11.

6. DISCUSSION

A total of nineteen experiments were carried out on micro - piles socketed onto a synthetic rock. Four experiments gave the load at the pile base from which shaft resistance and the end bearing could be determined at failure. However, only one of these four experiments gave a stress distribution along the pile. Three experiments gave the total – displacement curve up to failure. Eight experiments gave load – displacement curve below the failure. No useful results were obtained from the four experiments.

The maximum average shear stress and the maximum end bearing could only be determined in the four experiments shown in Table 3. These values have been used to determine the adhesion factors α shown in Figure 23, plotted against the unconfined compressive strength.

The Adhesion factor (α) that was measured for the rough socket is relatively high compared with the values to be expected from the empirical relationship, based on field load tests. The ratio between the unconfined compressive strength and the maximum end bearing stress varied from 1.5 to 5.5.

Exp. No.	unconfined compressive strength qr (MPa)	Peak average shear stress MPa	Adhesion factor, alpha α	Base stress at failure MPa	Ratio between qr and the maximum end bearing stress
2	4.85	2.5	0.515	16.4	3.4
3	5.32	3.31	0.622	8.0	1.5
4	2.10	1.33	0.633	11.5	5.5
11	3.80	0.84	0.221	11	2.89

the shear stress profiles at pile failure produced by the finite element analysis and the experimental result in laboratory is given in Figures 22.
The load distribution curve from the experiments and from finite element analysis for experiments shows very good agreement as can be seen from Figures 19. The end bearing capacity was 8.53 kN. The figure also shows that in the elastic range the ratio of load Qb/ Qt being carried to the base of the socket, was 34%, whereas the values predicted by the elastic solution was about 18 %.

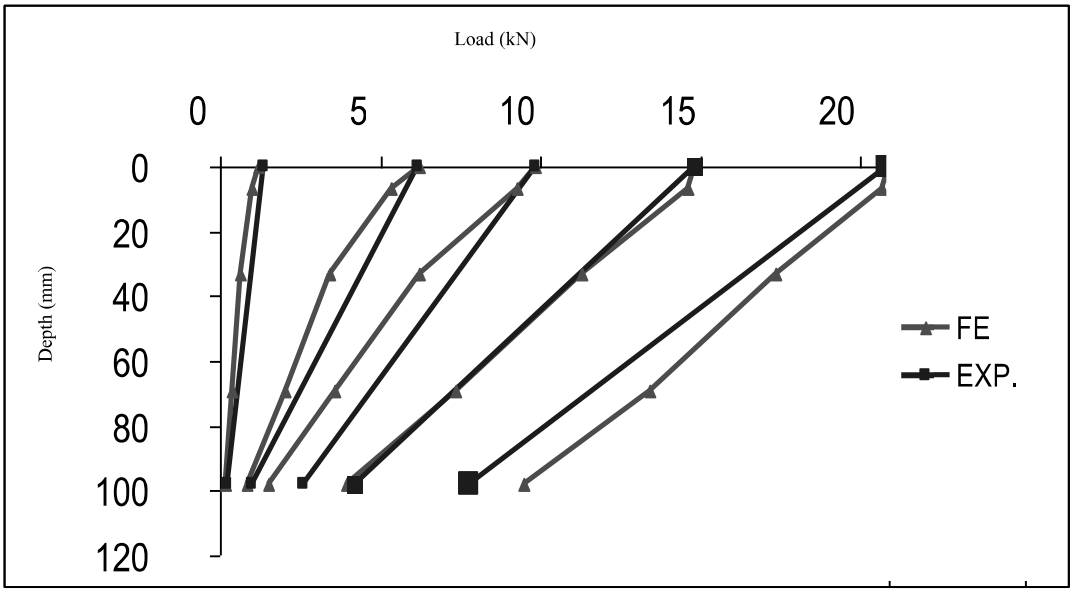

Figure 21. Comparison between the load distribution curves produced by Finite element (F.E.) analysis with experiment 4 results.

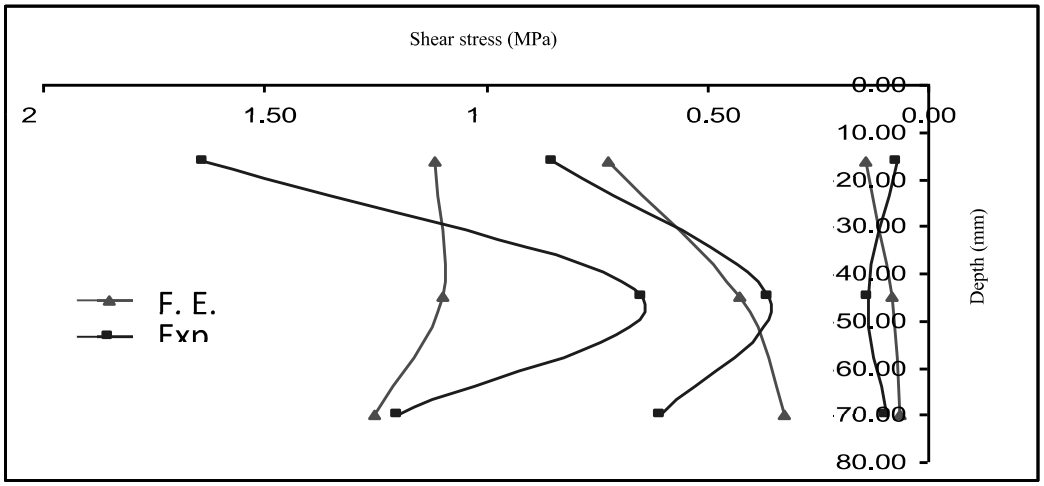

Figure 19. A. Geometry of the model rock socketed piles. **B.** Geometry model in PLAXIS **C**. Finite element mesh

The mesh generation is an automatic procedure in PLAXIS, in which the geometry is divided into a 15 – node triangular elements. The finite element programs calculate the displacement at the nodes and the stress at individual Gaussian integration points (or stress points). A 15 – node triangular element contains 12 stress points. Figure 19. C shows the finite element mesh of the rock-socketed model. A coarse mesh was selected to the model. In order to model the pile part more accurately a fine mesh was used. Figure 20 shows example of the load – displacement curves; that predicted by the finite element analysis, and that measured in the laboratory.

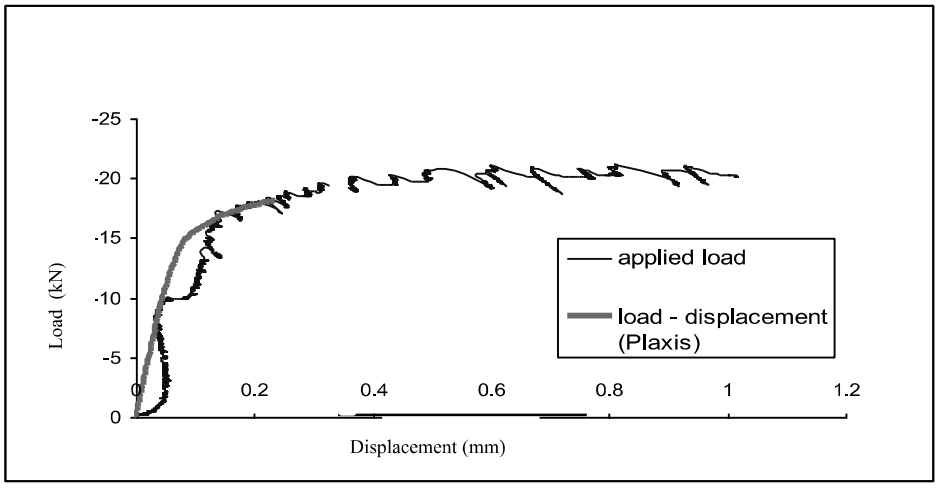

Figure 20. Comparison between the load displacement curve produced by Finite element (F.E.) analysis and the load displacement curve produced by experimental in the laboratory.

The load transfer behaviour along the pile and the pile base may be examined using the load distribution curve, this curve shows the changes in the axial load with depth. Figures 21, show an example of the comparison between the finite element and experiment. The curves from experimental data were determined from measurements of the applied load at the top of each pile, the axial strain in the concrete at different points of the experiment section, and the end-bearing load at the pile base. An example of the comparison between

assist in the interpretation of the experiments results. The finite element analysis was based on the laboratory-determined properties of the synthetic rock and used a simple Mohr-Coulomb model for the rock. The geometry of the numerical model and the boundary conditions are shown in Figure 19.A and B. Axisymmetrical analysis was used with the boundary conditions. The socket length and the socket radius are varied from one model to the other depending on the geometry of the experiment being modelled.

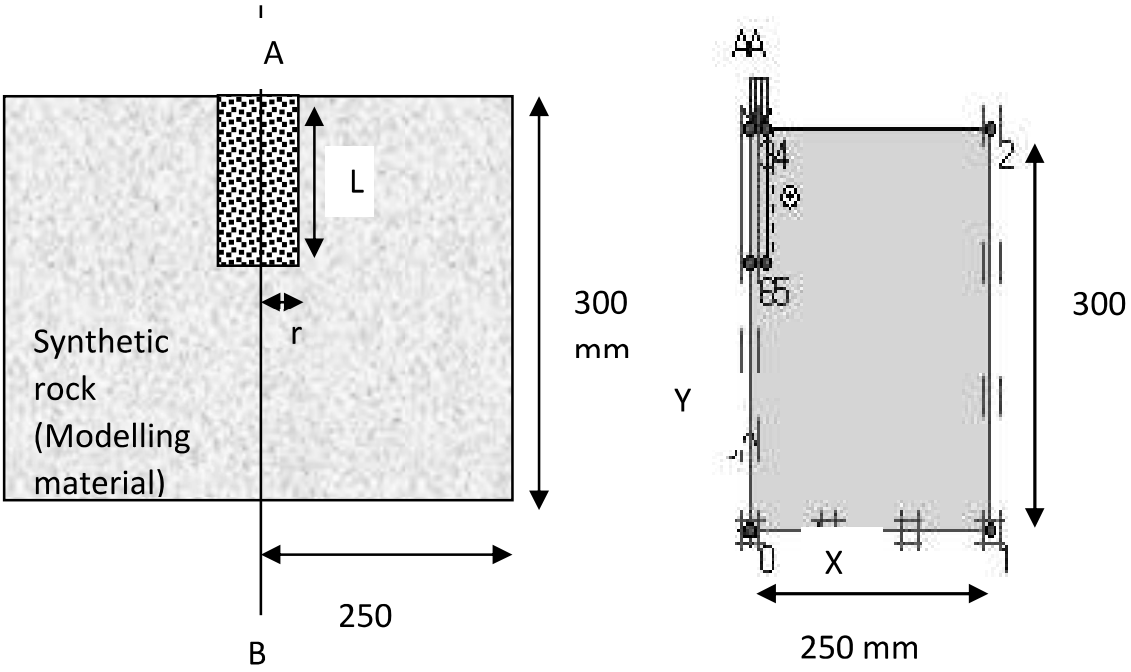

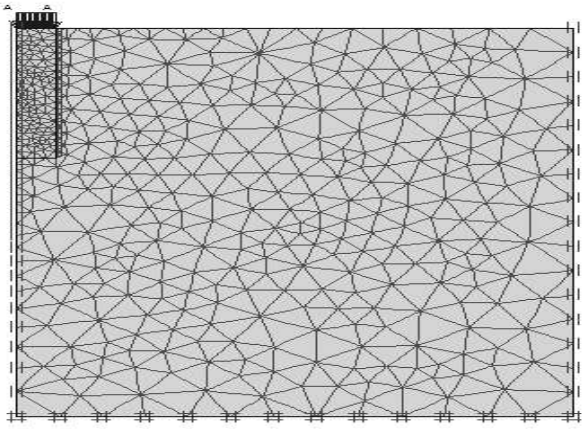

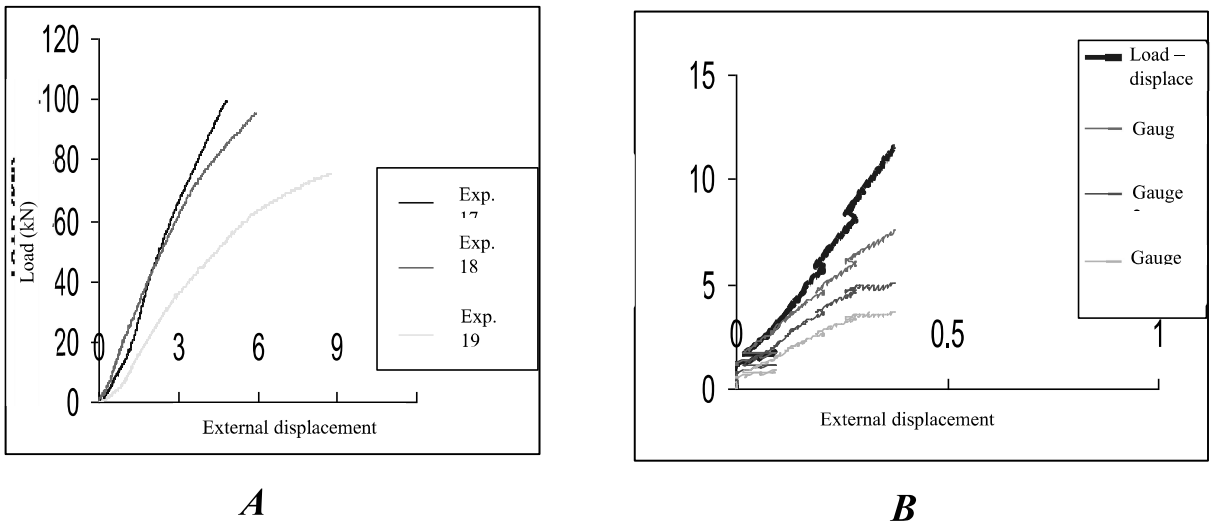

A *B*

Figure 17.A. Load displacement curve. Experimental 17, 18, 19. **B.** Load - External displacement curve and the load at different location inside the pile for experiment 16.

Figure 18. Pictures show experiment 18 after the test finishing, and the

5. Numerical modelling of rock socketed piles

A finite element analysis of the simulation of a rock-socketed pile was carried out using the PLAXIS computer programme in order to

effect of socket ratio. These four experiments where conducted with different socket ratio, (2.46, 2.21, 2.99, and 3.59). Unfortunately, these experiments were terminated earlier than would have been desirable because of pile head failure as the previous experiments. So far eight experiments had a pile head failure, and the pile properties used in experiment 16 are similar to the experiments 17, 18, and 19, so the pile head failure will happen again. For this reason, it was necessary to support the pile head from failure; in this context a steel ring was lubricated and placed around the pile head in the next experiments as shown in Figure 16. Figure 17.A. shows the load – external displacement curve for experiments, 17, 18, and 19. The load – external displacement curve with an example of the load measured in different points along the pile is given for experiment 16 in figure 17 B. This result shows that the strain gauges response was good up to a certain level which is similar to that level were the pile head started to fail. The steel ring also effects the load displacement curve because the ring was pushed down into the surrounding area of the pile head making as a support to the pile as shown in Figure 18.

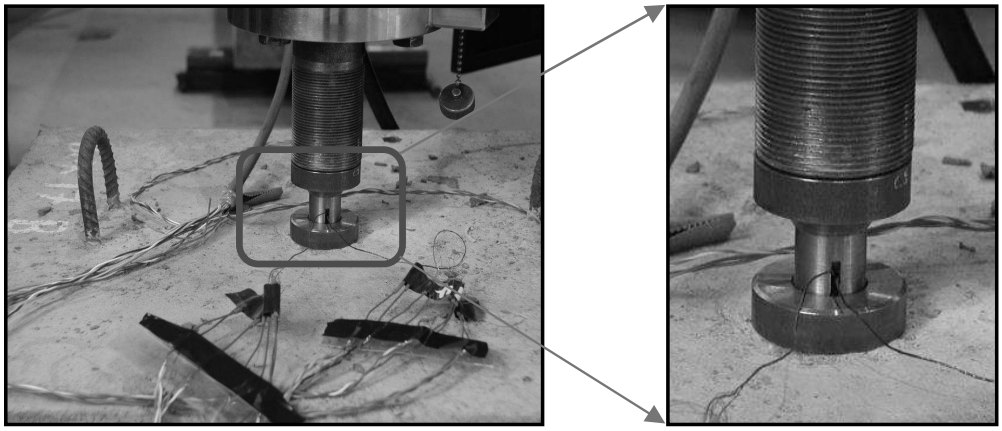

Figure 16. ***The steel ring around the pile head in experiment 19.***

Figure 14. A. Loading apparatus for the experiment 11. **B.** The pile head failure in experiment 15 Before testing. **C.** After testing showing the pile head frailer.

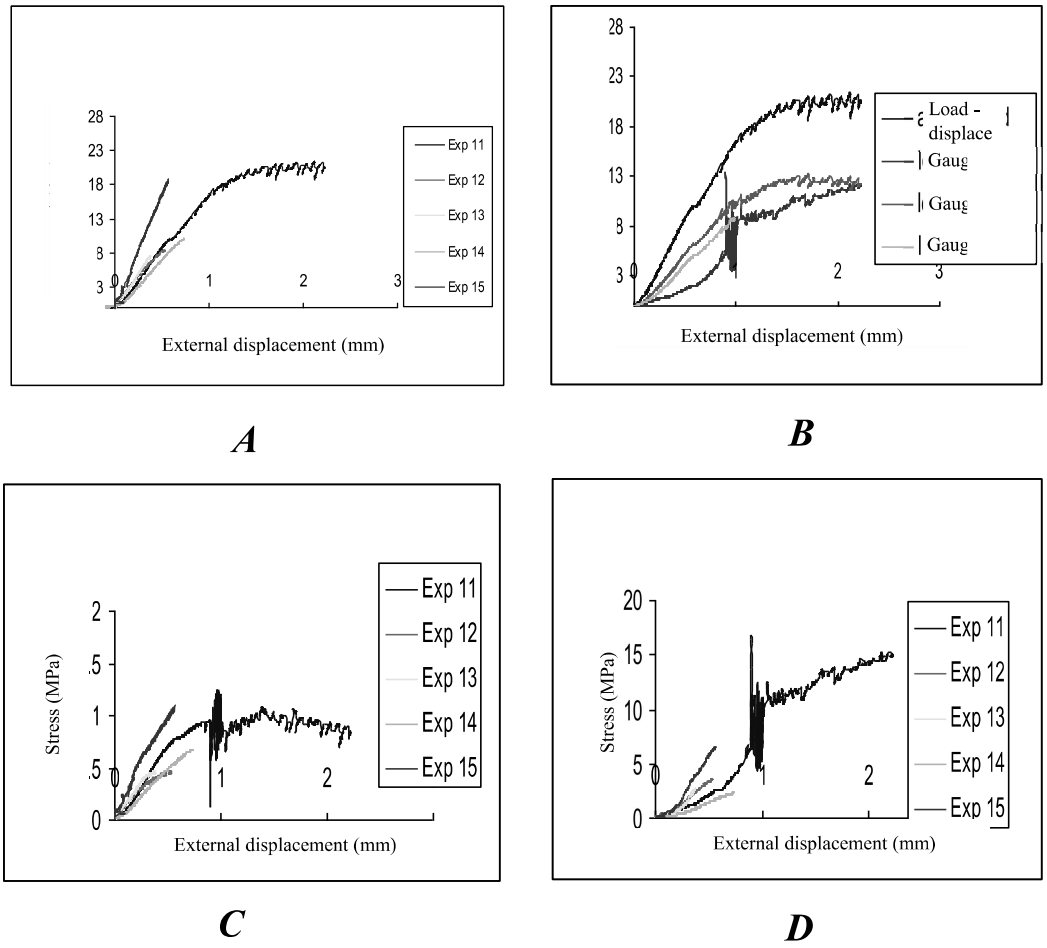

Figure 15.A. Load- External displacement curve. Load at different location inside the pile. Experiments, 11,12, 13, 14, and 15. **B.** Load- External - displacement curve. Load at different location inside the pile. Experiments 11. **C.** Side shear stress versus pile top displacement. Experiments, 11, 12, 13, 14, and 15. **D.** End bearing versus pile top displacement. Experiments, 11, 12, 13, 14, and 15.

Experiments 16, 17, 18 and 19 have the same mechanical properties for the synthetic rock with an unconfined compressive strength about 8.4 MPa. Table 2 contains the physical and mechanical properties of the test member and the pile properties. These four experiments that have the same properties were conducted in order to investigate the

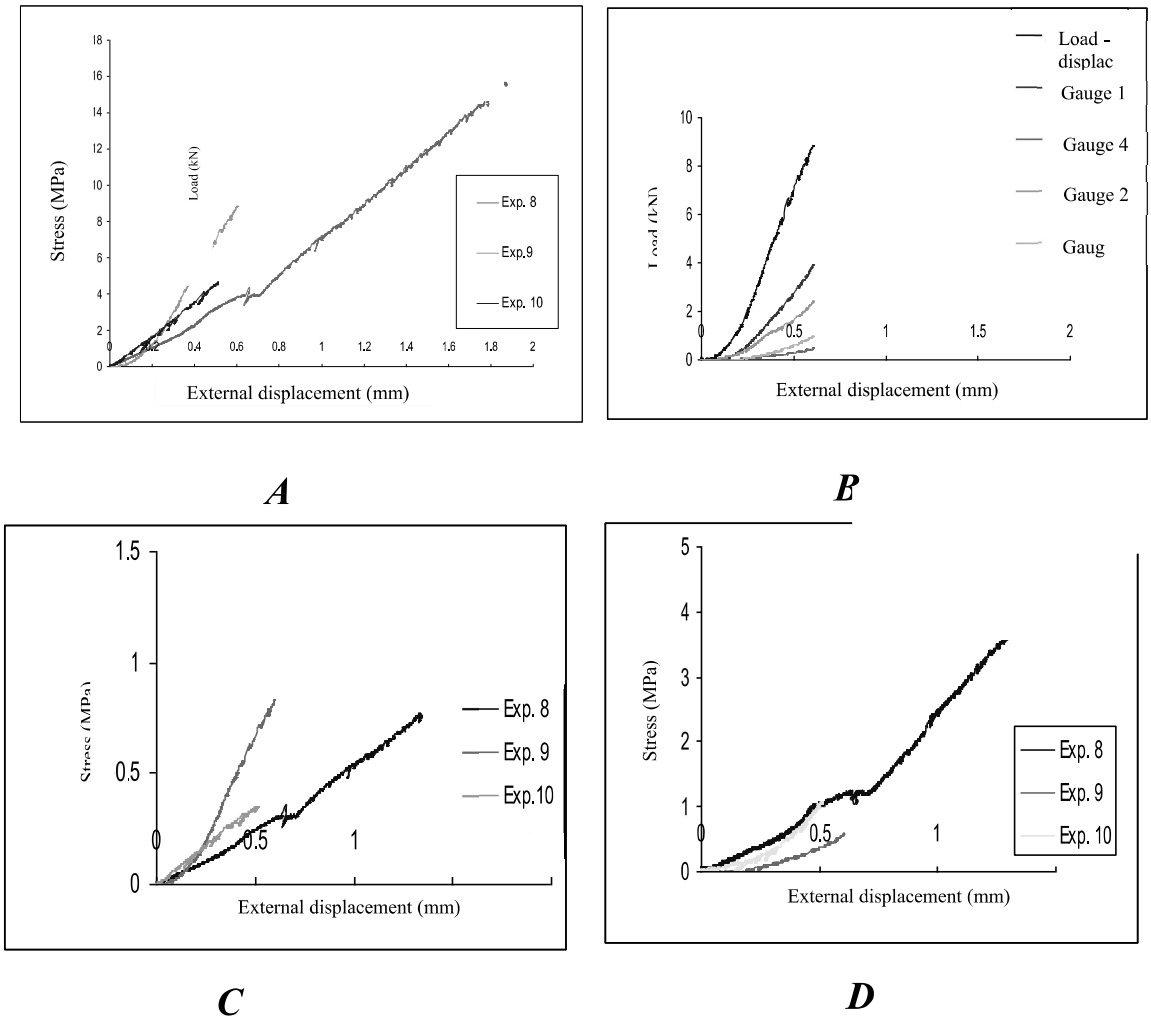

Figure 13. A. Load- external displacement curve. Load at different location inside the pile. Experiments 8, 9, and 10. **B.** Load- external displacement curve. Load at different location inside the pile (Experiment, 9). **C.** The side shears stress, for experiments 8, 9, and 10. **D.** The base stress for experiments 8, 9, and 10.

Experiments. 8, 9, 10, 11, 12, 13, 14 and 15. These eight experiments were divided into two groups. The first group comprise of experiments, 8, 9, and 10, where the side wire system was used. The second group includes experiments, 11, 12, 13, 14, and 15, where the central wiring system was used to avoid cut-off for the wires as a result of the shear force between the pile and the synthetic rock. Among the three experiment 8, 9, and 10 (as indicated by Table 2) experiment 9 has the highest unconfined compressive strength of all experiments with an unconfined compressive strength (qr) about 22.75 MPa. Both experiments 8, and 10 have similar unconfined compressive strength 2.47 - 2.54, but experiment 8 has a lower Poisson's ratio 0.165 compare with experiment 10 which has a value of 0.297. Unfortunately, all the three experiments were not completed because of pile top failed. Figure 13A; show the load – external displacement curves for experiments 8, 9, and 10. An example of the typical results of the load – external displacement curve and the load measured in different points along the pile for experiments 8, 9, and 10, is shown in Figure 13 B. The side shear stress, and the base stress versus the pile top displacement for experiments 8, 9, and 10 is presented in Figures 13 C, and 13 D. The second group comprise experiments, 11, 12, 13, 14 and 15, where the central wire system has been used. The general view for the experiment 11 is shown in Figure 14 A. All these experiments were terminated before the actual finishing of the experiment because of pile head failure; except experiment 11 was completed until the end of the experiment without any failure to the pile head. Figure 14 B and C shows the pile head before and after failure in experiment 15. Figure 15 A shows the load – external displacement curves for experiments, 11, 12, 13, 14, and 15 respectively. Figure 15 B also shows that the central wire system has significant effect on the strain gauges reading as the gauges are reading until the total failure of the pile. The side shear stress versus the pile top displacement for experiments 11, 12, t13, 14 and 15, is given in Figure 15 C. The end bearing versus the pile top displacement for experiments 11, 12, 13, 14 and 15 is given in Figure 15 D.

Figure 11.A. Load- external displacement curve experiments 1, 2,3,4,5 and 6. **B.** Load- external displacement curve experiment 4. Load at different location are also shown. **C**. Side shear stress experiments 2, 3, and 4. **D.** Base stress experiments 2, 3, and 4.

4.2Experiments conducted with grooved steel bar

Experiment 7 is the first Experiment which used the grooved steel bar. The load displacement curve and the load at three different levels inside the pile are shown in Figure 12. This figure shows the improvement in the strain gauges reading compared with the first six experiments. The side shear resistance and the end bearing versus the pile top displacement cannot be plotted because the strain from the gauges at the bottom of the pile stopped from reading just as the experiment started as shown in Figure 12.

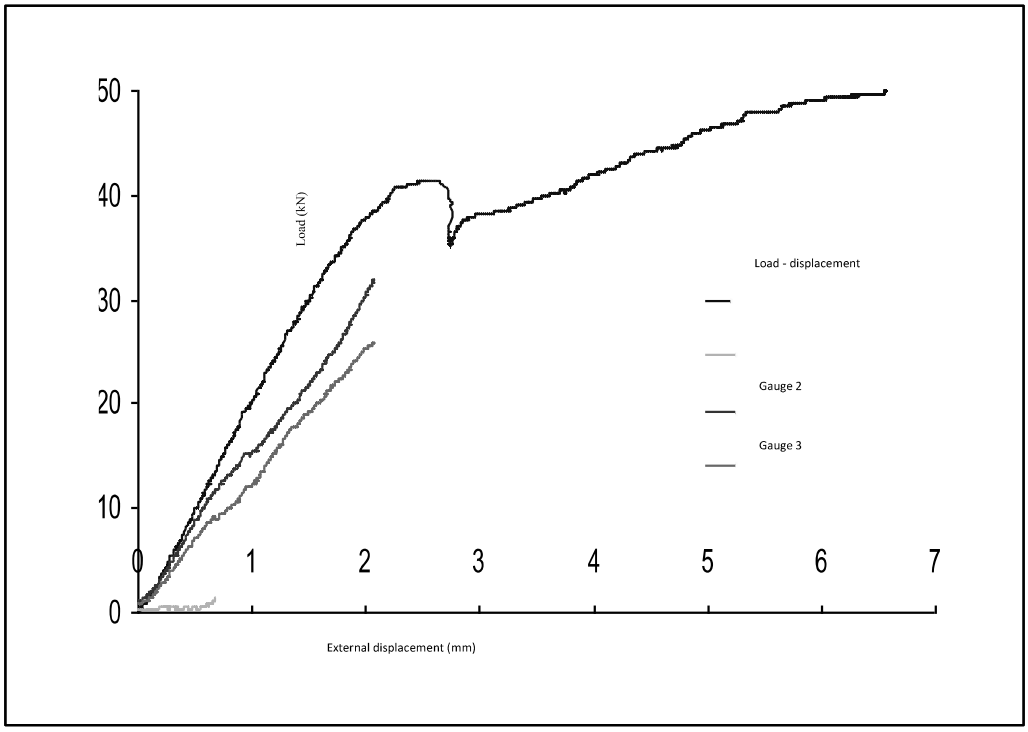

Figure 12. Load- external displacement curve. Load at different location inside the pile for Experiment 7.

comparison between load – displacement curves for these six experiments which, shows that pile head failure occurred only in experiment one whereas all the other five experiments were completed without pile head failure. An example of the typical results of the externally measured load – displacement curve and the load measured in different points along the pile for experiments 4 is shown in Figure 11.B. In all of these six experiments the some of the strain gauges gave unusual results and were considered to be unreliable. The results of these gauges could not be used to interpret the load distribution along the shafts. However, by assuming a good response from gauge at base of the pile in experiments 2, 3, and 4, the shear stress, and the base stress versus the pile top displacement are given in Figures 11.C. and 11.D.

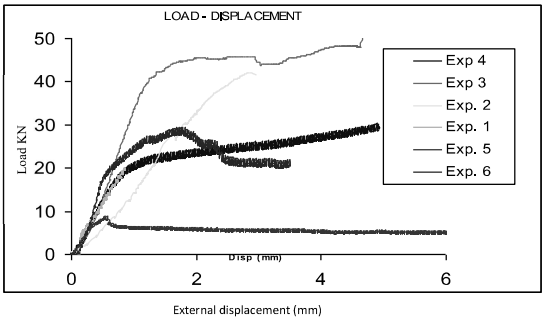

B

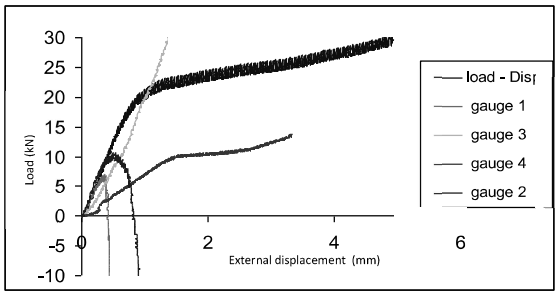

A

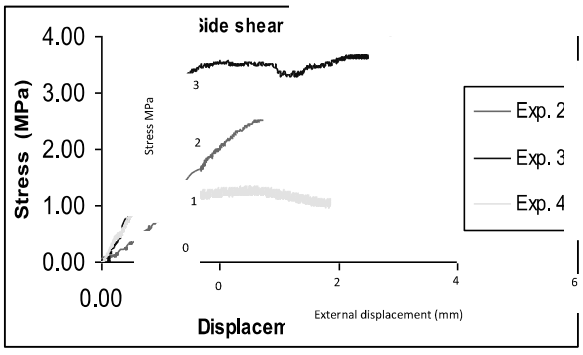

D

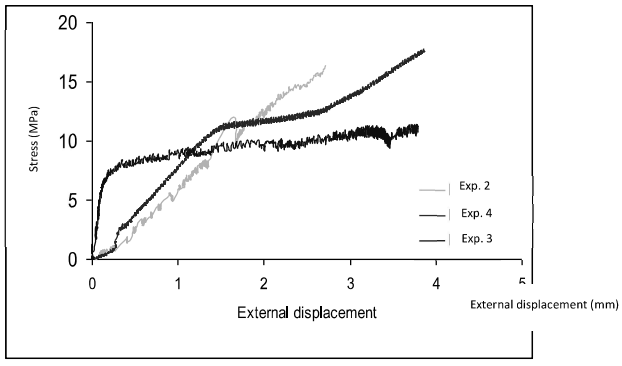

C

Figures 9. A and **B** shows an example the position of the stain gauges used in the experiments that used the grooved steel bar and the smooth steel bar respectively.

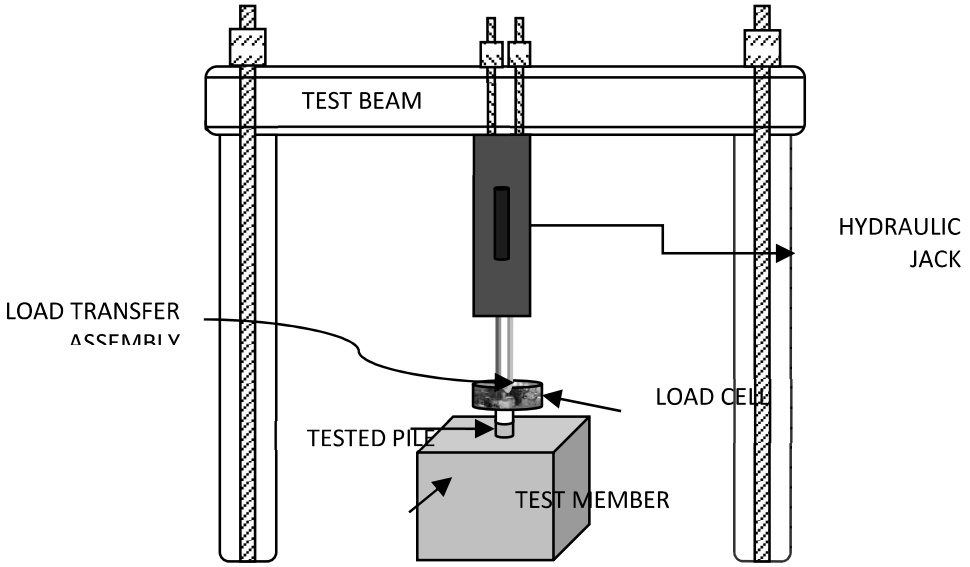

Figure 10. General view of the load test.

4. Experiments results

4.1 Experiments conducted with smooth steel bar

The experiments conducted with the smooth steel bar include; experiments 1, 2, 3, 4, 5, and 6. Table 2 summarize the physical and mechanical properties of these six experiments. The first experiment was constructed with three steel bars, with five strain gauges on one side of each bar. Unfortunately, the first experiment was terminated early (20.31 kN) because of the collapse of the pile top at 22.65 MPa, which is just 33.3 % of the failure stress of the concrete (68 MPa). The pile for the experiments 2 and 3 was cast in the same time. In both experiments just two plates were used with strain gauges on one side of the steel plate. In experiments 4,5, and 6, only one plate with two strain gauges on two sides was used. Figure 11. A which give a

A B C

Figure 8. A. Smooth a steel plate. **B.** Grooved steel bar. C. The steel bar dimension

Figures 9. A and B shows an example the position of the stain gauges used in the experiments that used the smooth steel bar and the grooved steel bar respectively.

The strain measured was converted to stress or load. Figure 10 shows the General view of the load test. The side shear stress and the end bearing stress for the nineteen experiments are presented along with the properties of the concrete of the pile and the externally measured load displacement curve.

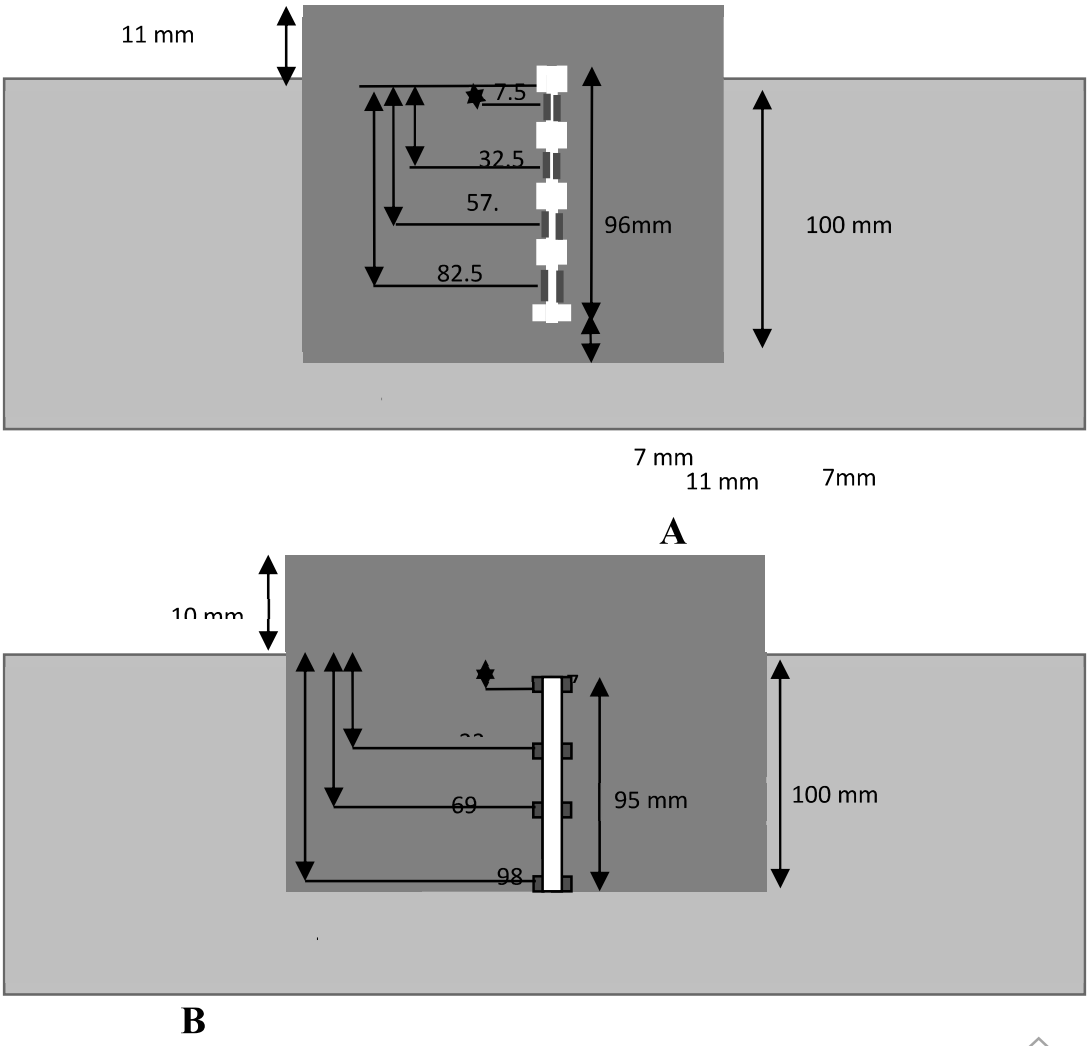

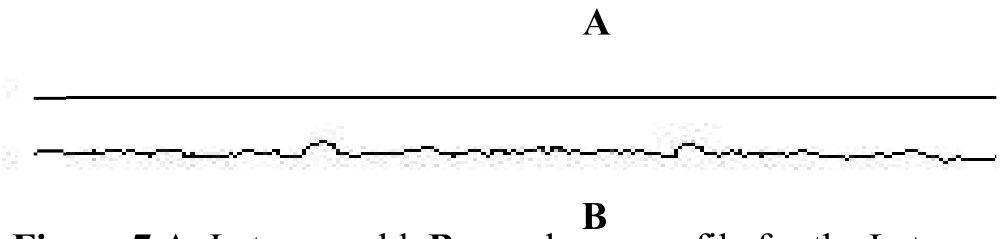

Figure 7.A. Latex mould. **B.** roughness profile for the Latex mould.

Electrical resistance Foil strain (E.R.S) gauges were used to measure the local strain at different levels along the model pile. Two different size steel bars were used inside the model pile. The first steel bar was as shown in Figure 8 A. This comprised of a smooth a steel plate with dimension of 5 mm in width, 0.5 mm in thickness. The length varies from 91 mm to 110 mm. The experiments conducted with the smooth steel bar include; experiments 1, 2, 3, 4, 5, and 6. These six experimental have different design in terms of the number of the steel bar inside the pile. Experiment number 1 used three steel bars whereas the experimental 2 and 3 used two steel bar and experiments 4, 5 and 6 used only one steel bar inside the pile. The second type is the grooved steel bar, as shown in Figure 8 B. This steel bar has dimension of 6 mm in width, and thickness as shown in Figure 8 C. The length of the grooved steel bar is 96 mm for experiments 7,8,9,10,11,12,13,14,15,17,18,19, whereas the length of the steel bar was 71 mm in experiments number 16.

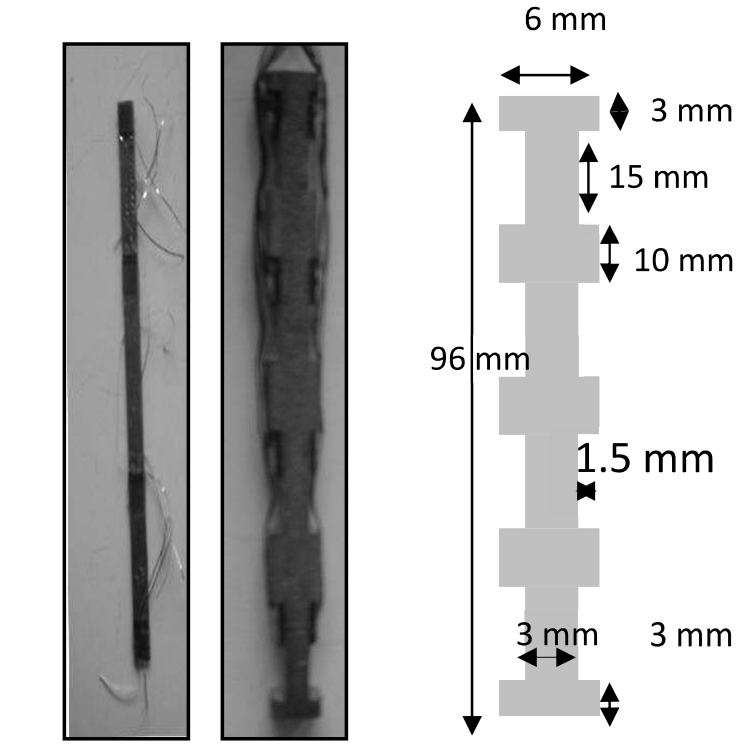

1. Experimental procedures and design

The equipment that has been used to carry out the model pile experiments, and the testing procedure adopted will be explained in this section. The socket was drilled in the centre of the test block. The diameter of the socket ranged from 24.1 mm to 45.2 mm. The lengths of the socket were 80 mm, 100, and 120 mm. A photograph of typical sockets is shown in Figure 6 A, B and C.

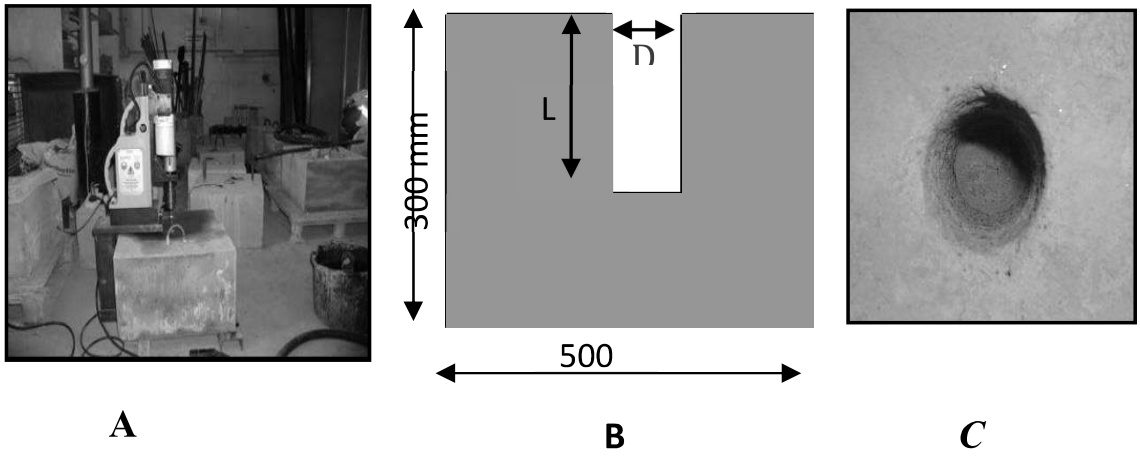

Figure 6.A. Drilling machine, fixed into a steel base
B shows the socket geometry. **C** shows the picture of the hole.

The socket wall roughness has a significant effect on the side shear resistance. For this reason, it was decided to develop a method of measuring the roughness. The roughness of the wall of the socket was moulded using a rubber material called liquid Latex. The Latex was brushed into the socket wall and after 5 days it becomes solid and can be pulled out. The surface of this material has a positive picture of the Roughness of the socket. This mould has been used to determine the socket profiles as shown in shown in Figure 7 A and B.

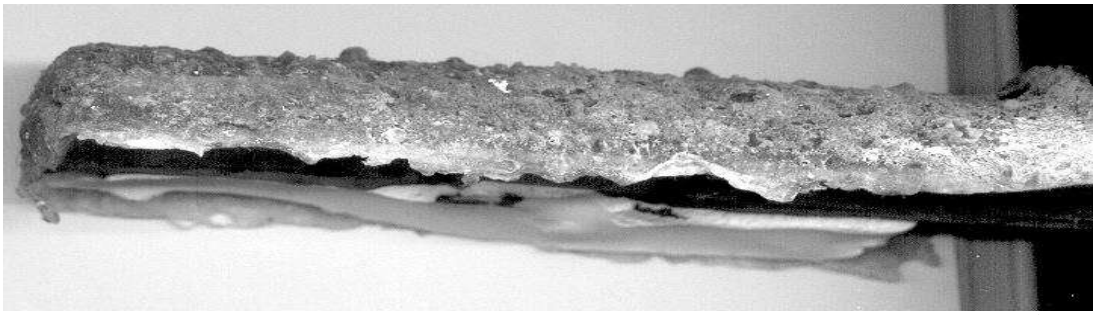

Table 2. The average of the unconfined compressive strength, Tensile strength and the Young's modulus of the modelling material and the concrete of the pile

Exp. No.	1	2	3	4	5	6	7	8	9	10	11	12	13	14	15	16,17, 18,19
The average tensile strength of modelling material (kPa)	-	579 .85	494 .38	178 .92	660 .35	355 .51	23 0	28 8	26 12	20 4	10 34	14 2	77 9	22 8	10 50	1259
The average unconfined compressive strength of modelling material (qr) (MPa)	9. 24	4.8 5	5.3 2	2.1	2.9 1	2.4 2	3. 55	2. 47	22 .7 5	2. 54	3. 8	1. 37	6. 81	3.0 2	5. 09	8.44
The unconfined compressive strength for the concrete that was used in the piles (qc) MPa	68 .0 0	64. 21	64. 21	68. 50	68. 50	68. 50	45 .8 1	46 .0 6	46 .0 6	46 .0 6	46 .0 6	46 .0 6	46 .0 6	46. 06	46 .5 0	46.5
Poisson's ratio of modelling material (Vr)	0. 19	0.1 6	0.1 6	0.1 5	0.1 6	0.1 5	0. 16	0. 16	0. 16 6	0. 29 7	0. 17	0. 17	0. 19	0.2 1	0. 17	0.18
Poisson's ratio for the concrete used in the piles (Vc)	0. 15	0.1 6	0.2 3	0.2 1	0.2 1	0.2 1	-	-	-	-	-	-	-	-	-	-
The tensile strength for the concrete that was used in the piles (σ t) MPa	4. 76	4.7 6	4.7 6	-	-	-	-	-	-	-	-	-	-	-	-	-
Young's modulus of modelling material. (Er) GPa	6. 00	6.7 2	6.2 9	4.2 5	2.9 2	4.2 5	4. 36 6	4. 29	15 .5 3	3. 03	3. 82	3. 2 5	8. 9 7	3. 3 3	8. 3 3	10.5
Young's modulus of the concrete (Ec) GPa	26 .0 0	28. 6	24. 00	27. 7	27. 7	27. 7	19 .9 0	19 .1	19 .1	19 .1	19 .1	19 .1	19 .1	19. 1	20 .1	20.1
Ec/Er	7. 36	4.2 6	3.8 2	6.5 1	9.5 0	6.5 1	4. 56	4. 45	1. 22	6. 30	5. 00	5. 88	2. 13	5.7 4	2. 41	1.92
The tensile strength of concrete (σt c) kPa	-	475 7	415 9	--	-	-	-	-	-	-	-	-	-	-	-	-

Figure 4. Measuring the Young's modulus for the cylinders of the simulated soft rock material, it shows also the computerized system.

A typical result is shown on Figure 5. For each test member three cylinders were tested, with three cycles of loading and unloading. The values that are given in Table 2 represent the secant modulus at an axial stress about 30 % of the ultimate strength.

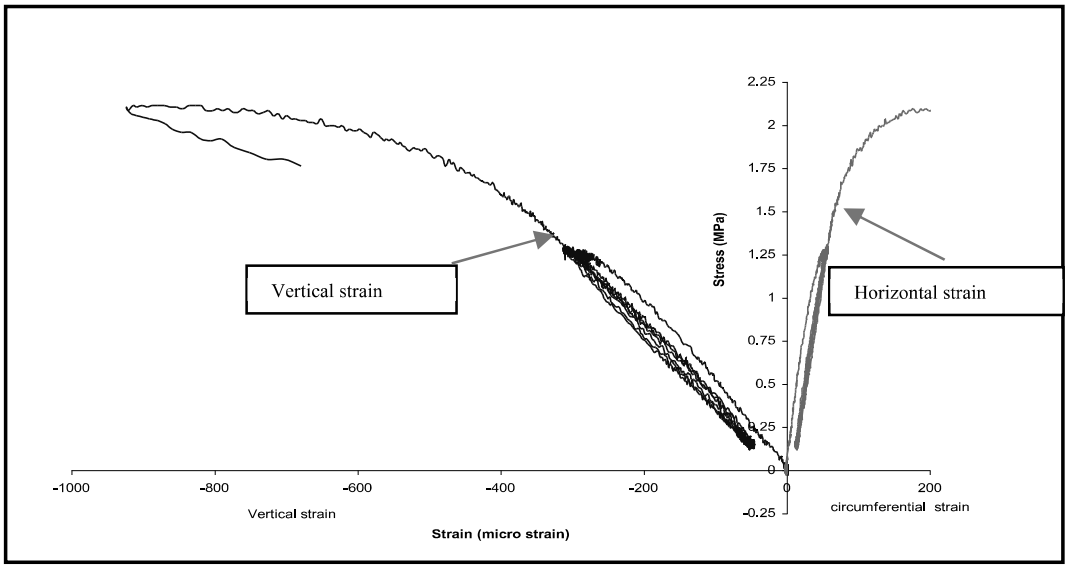

Figure 5. Stress strain behaviour for simulated rock material, Experiment 12.

When the specimen undergoes compression, it is shortened and this generally is accompanied by an increase in its cross-sectional area. The ratio of lateral deformation to linear deformation, within the elastic limit, is known as Poisson's ratio of modelling material (Vr).

The compressive strength of the simulated rock was determined by loading a 100 mm cube to the failure using a testing rate of 0.6 MPa / sec, which is in, range of (0.5 to 1 MPa / sec.) as suggested in the International Society for Rock Mechanics (I.S.R.M.). The modelling material have a range of unconfined compressive strength between (1.3- 22 MPa), Table 2 shows the unconfined compressive strength for different modelling material.

Table 1. Different types of mixing that used to simulate the soft rock. The materials that used are shown by percent of weight.

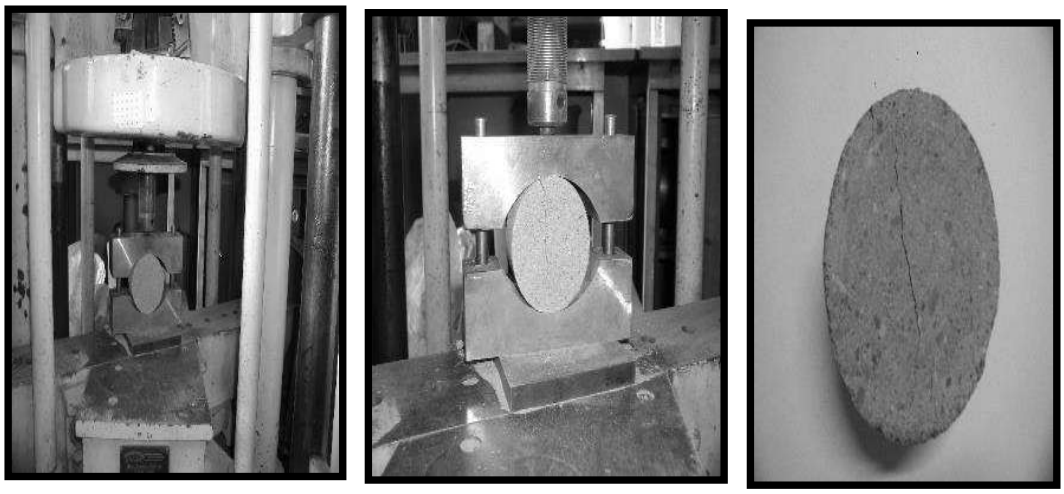

Figure 3. Brazilian test for rock simulated material

The Young's modulus is the most important of the elastic constants and can be derived from the slope of the stress - strain curve obtained when a rock specimen is subjected to unconfined compression, it being the ratio of stress to strain. The common method of measuring the Young's modulus is to test a core under uniaxial compression, with a length to diameter ratio of 2. The ends of the specimen were ground to be parallel to the test machine's platens to minimize the development of stress concentrations at the ends of the sample. Four strain gages were bonded to the cylindrical specimen, two in the vertical direction parallel to the cylinder axis, and the other two in the circumferential direction. The strain readings and the load were recorded using computerized system, as shown in Figure 4.

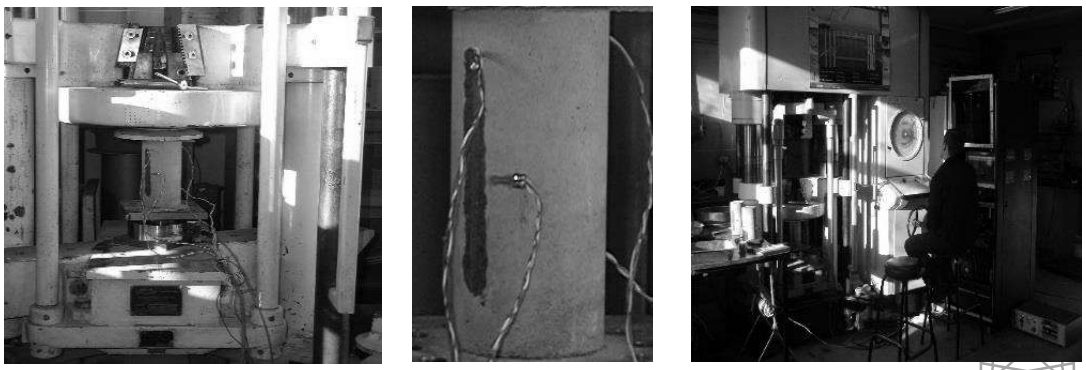

test member was stored in a room with normal environmental conditions.

A series of laboratory experiments have been made in order to determine the mixing properties for the test members. These tests include the unconfined compressive strength, Young's modulus, and tensile strength. Brazilian test method was adopted to measure the tensile strength. The test consists of compressing a circular solid disc to failure as shown in Figure 3. The Brazilian test is only valid when primary fracture starts from the centre spreading along the loading axis Lama and Vutukuri, (1978 a). In the laboratory a cylinder from each mix was cut into three discs with a thickness approximately equal to the specimen radius, (50 mm thickness, 50 mm radius) as recommended in Brown, E.T. (1981). The discs were placed in an apparatus, designed to carry out Brazilian test, the samples were loaded continuously with testing rate of 0.6 MPa / sec. Table 2 shows the inferred tensile strength for the different modelling material tested.

Experiments No.	Sand %	Water %	Cement %	P.F.A. %	Lime %	Bonding Plaster %	Mixing Name
1	78.8	11.6	9.6	-	-	-	A
2	76.1	14.6	4.7	4.6	-	-	B
3	83.9	9.3	6.8	-	-	-	C
4	79.0	14.0	4.8	-	2.2	-	D
5	-	36.8	-	-	-	63.2	E
6	73.8	16.1	3.5	6.6	-	-	F
11	-	29.8	-	-	-	70.2	G
12	80.2	13.1	4.2	-	2.5	-	H
13	74.9	15.4	9.7	-	-	-	I
7	79.5	13.9	6.6	-	-	-	J
14	75.2	15.4	4.6	4.8	-	-	K
8	74	18.5	7.4	-	-	-	L
9	69.5	14.6	15.9	-	-	-	M
10	73.3	14.7	4.3	-	7.7	-	N
15	73.3	15.9	10.8	-	-	-	P
16, 17, 18, 19.	72.5	20	7.5	-	-	-	O

because of their effect on the material strength. An example of the particle size distribution for the sand used in the simulated rock materials is given in Figure 2. Table 1 shows the different types of materials used to simulate the soft rock.

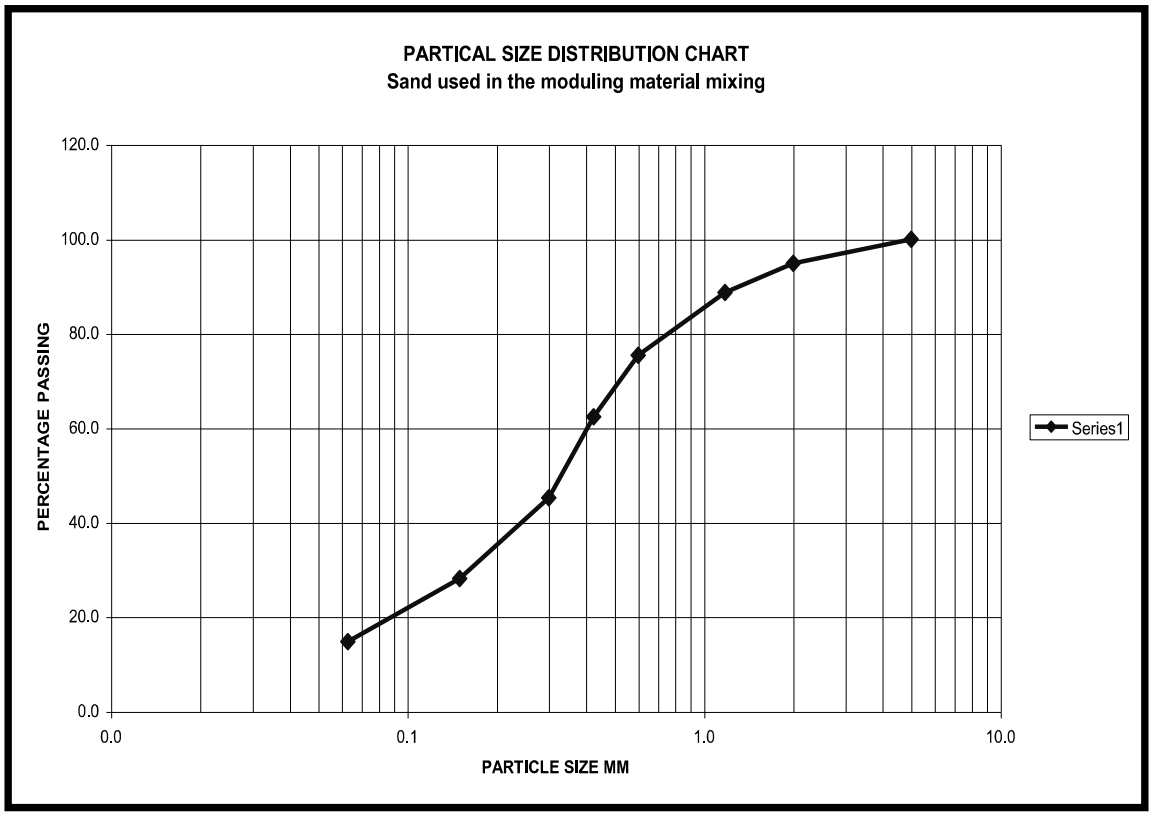

The material was prepared in a mixer with maximum capacity about 0.08 . The material was mixed in two batches, and the mould was filled in two layers. In order to obtain a dense material, the material was compacted for 5 minutes using a poker Vibrator.

Figure 2. Particle size distribution chart for the sand used in the modelling materials.

After filling the wooden mould, the specimen was cured for 28 days before being drilled and the pile being cast. The pile was allowed to cure for another 28 days before being tested in the laboratory. The

Numerous materials have been used in the past to simulate the rocks; these materials include cork, plastic, concrete, plaster, Portland cement mortar, pumice, rubber, and gelatine. Powdered natural soft rock has also been used by Lam and Johnston, (1989) to model the soft rock or even to model the stronger rock. These materials have been used with cementing agents such as Portland cement, gypsum cement, natural cement, and pottery clay. Rosenbland (1968) states that the most used are the Normal Portland cement and gypsum cement. The filling material that has been used to alter or control the properties of the mode material are, sand, lime, kaolinite. Some other materials have been used as additions to provide specific characteristics such as sugar and tannic acid. The cement agents that have been used in this study are Portland cement, and bonding Plaster.

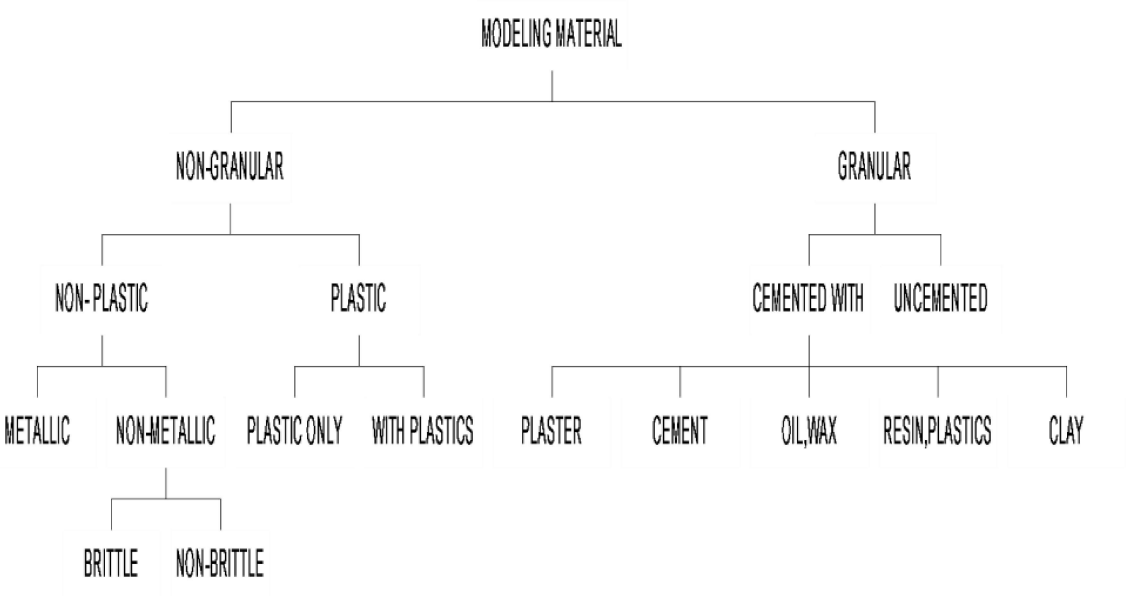

Figure 1. Classification of the modelling material. Stimpson, B. (1970).

The most important filler material is the sand, because it is used to provide the angle of friction for the material. The sand has been used as a filling material. The other materials which have been used are the pulverised fuel ash (P.F.A), and lime. These materials are used

roughness of the socket wall on the peak side shear resistance, and on the load distribution between the shaft and the base of the pile. In this context an experimental programme was conducted in which small-scale concrete piles were loaded under compression. All the piles were instrumented internally by strain gauges glued onto a steel bar. The values of the strain were recorded to obtain the strain distribution at different elevations inside the pile. In order to investigate the effect of the unconfined compressive strength of the rock, a number of experiments were conducted with different unconfined compressive strengths within the range from 1 to 22 MPa. The effect of the socket geometry was investigated in, six experiments with the same property of rock and concrete but with different lengths and diameter of pile. The roughness profile of the side of the piles was obtained in all the experiments.

2. Simulation of the rocks and soft rock properties

In order to model the rock-socketed piles in the laboratory it is necessary to simulate the natural weak rock in which the pile is to be embedded. In this section presents the properties of the modelling materials which have been used to simulate the weak. According to Rosenblad (1968) the modelling material should be economical, easily obtainable and repeatable; it also should be similar to the rock in all of its pertinent properties. Two other important factors are that the static properties should not change with time and that it should be possible for measuring instruments to be easily attach or embedded in the material. Wide ranges of modelling material are used to simulate different physical properties of the material. Stimpson (1970) classified the modelling materials into two main groups, granular and non-granular as shown in Figure 1. The suitability of the model material is frequently founded on the success with which one property only satisfies similitude such as uniaxial compressive strength, tensile strength or shear strength Stimpson (1970).

fall within this category. The economic design of deep foundations can be a significant aspect of many projects. The deep foundations include timber piles, steel piles, pre-cast-concrete piles, and cast-in-place piles. The piles can be placed singly or in groups. The concrete piles are generally more durable than steel and wooden piles. The concrete piles can be pre-cast or cast in place. Piles can be bored to the top of the rock or can be extended into the rock to act as the rock-socketed piles. The economic growth in recent years has led to an increase in the use of rock-socketed piles due to the requirements for higher structural load capacities.

Based on the method of the load transfer from the pile to the surrounding ground, the piles can be classified into end bearing piles, side wall shear resistance only (skin friction) piles, or as a combination of end bearing and side shear resistance. Rock socketed piles derive their capacity from two components, the shaft friction and the base resistance. These socketed piles have an advantage over piles which achieve their capacity from end bearing only as skin friction achieved at the rock/pile interface increases the load capacity of the pile and also because it spreads the load deeper into the rock, thus reducing the risk of overstressing locally weak layers under the pile tip.

The design of piles socketed into rock is traditionally based on local knowledge derived from observation of full-scale static load tests, empirical factors related to the unconfined compressive

strength of intact rock, or conservative city or state ordinances. The development of computer power has contributed to shifting the design of rock-socketed piles from empirical methods toward a theoretical method.

The aim of this paper is to study the effect of different factors, such as unconfined compressive strength, socket geometry, and the

الملخص

تم اجراء سلسلة من التجارب المعملية على مجسمات معملية للأساسات الخرسانية المحفورة بالصخور (الركائز الصخرية) لاختبار مدى دقة العلاقات التجريبية المستخدمة والمعتمدة على العلاقة بين قوة الصخور وقدرة الصخور على استيعاب الحمل. تم تحميل هذه الاساسات الخرسانية الصغيرة بحمل راسي وحفرت وأسست في تجويف صخري من الصخور الصناعية بحيث تمل هذه الصخور فيئة الصخور الضعيفة. قيمة الاجهاد تم تسجيلها بداخل الركائز الصخرية الخرسانية على ارتفاعات مختلفة كذلك تم مقاومة الصخور عند القاعدة. كما تم تحديد مقاومة القص الجانبي والمقاومة عند القاعدة الاساسية في هذه التجارب. يعتبر التنبؤ بمقاومة القص الجانبية من خصائص الصخور وخصائص الاساسات امراً في غاية التعقيد. وتربطها الطرق الحالية بشكل تجريبيي بمقاومة الضغط غير المحصورة لكتلة الصخور (qr). تمت مواجهة صعوبات في تطوير تجارب الركائز الصخرية النموذجية للحصول على المعلومات المطلوبة. ولكن لم يكن ممكننا الوصول الى استنتاجات نهائية نتيجة للصعوبات التي واجهت التجارب، على اية حال النتائج تدل تشير النتائج إلى أن عامل الالتصاق كان حوالي 0.6 في التجويف الخشن، بينما في التجويف الأملس كان عامل الالتصاق حوالي 0.22. تراوحت العلاقة بين أقصى مقاومة لحمل النهاية وقوة الضغط غير المحصورة للصخور بين 1.5 إلى 5.5 مرة لمقاومة الضغط غير المحصورة للصخور.

1. Introduction

Deep foundations are required when there is no stratum of sufficient strength and stiffness that can support the required structural loads of a building within an economic depth. Deep foundations generally imply piled foundations, although caisson or shafts sometimes would

Laboratory investigation into the performance of rock socketed piles in synthetic weak rocks

Salah Musa Elgarmadi. Geology and Environmental Science Department, Faculty of Science, AL-Elmergib University
Ali Elsaeh Enbaia Petroleum Engineering Department, Faculty of Engineering, Alrefak Private university
Majed Alsadeg Alnfes . Geology and Environmental Science Department, Faculty of Science, AL-Elmergib University

Abstract

A series of laboratory experiments on small scale rock socketed concrete micro-piles were made to investigate the reliability of published empirical relationships between the strength of the rock and the capacity of the rock to take the pile load. These model piles were axially loaded and socketed into synthetic rock, the properties of which were chosen to simulate weak rock. The values of the strain were recorded to obtain the distribution at different elevations within the pile. The side shear resistance and the base resistance were determined in these experiments. The prediction of the shaft resistance from the rock and the pile properties is a complex problem. The current methods are empirically related to the unconfined compressive strength of the rock mass (qr). Difficulties were experienced in developing the model rock socket pile experiments to obtain the required information. But it is not possible to make definitive conclusions due to difficulties with the experiments; however, the results do indicate that the adhesion factor was about 0.6 in the rough socket, whereas in smooth socket the adhesion factor was about 0.22. The relationship between maximum end bearing resistance, and the unconfined compressive strength, varied between 1.5 to 5.5 time's unconfined compressive strength.